PHARO (Palomar High Angular Resolution Observer): A dedicated NIR camera for the Palomar adaptive optics system

B. Brandl, T. L. Hayward, J. R. Houck, G.E. Gull, B. Pirger, & J. Schoenwald

Center for Radiophysics and Space Research
Cornell University

ABSTRACT

We describe Cornell's NIR camera system for the Hale 200" telescope adaptive optics system at Palomar Observatory. The instrument is under construction at this time, and we expect first light at the telescope in December 1997. Here we summarize the camera's design as well as its expected performance.

Keywords: Adaptive Optics, Instrumentation, NIR camera, grism spectroscopy, coronography, HAWAII array

1. INTRODUCTION

JPL and CalTech are building an adaptive optics (AO) system[1] for the f/16 Cassegrain focus of the 200" Hale telescope on Palomar mountain. First test results are expected during 1997. As part of Cornell's contribution to the Palomar collaboration, we will provide the NIR science camera for this system.

The boundary conditions for the camera were primarily the telescope optics (f/15.64 beam) and the available space on the AO optical bench. The design goal was to provide the best possible images at the diffraction limit throughout the 1 – 2.5 μm wavelength range where the AO system will operate most effectively, while maintaining sufficient flexibility in the optical configuration to accommodate varying atmospheric conditions and the expected wide range of observing projects. To meet this goal, the camera is equipped with two different imaging modes: one with a 0.025"/pixel scale which sufficiently samples the diffraction disk at the shortest wavelength (J-band), the other with a 0.040"/pixel scale which still provides sufficient sampling at longer wavelengths (H- and K-band). For a detector we chose the new 1024×1024 "HAWAII" HgCdTe array manufactured by Rockwell, resulting in a field of view of 41" × 41" in the low resolution mode. Larger pixel scales wouldn't be advantageous because of the limited isoplanatic angle.

In addition to the standard J, H, and K filters, there will be a set of common narrow-band filters for low resolution spectroscopic work, plus three grisms which cover the J-, H-, and K-bands with a spectral resolving power $\lambda/\Delta\lambda$ between 1000 and 1500. (The scientific benefits of using spectroscopy within an AO-system are illustrated by a recent study of the planetary nebula IC418[2].)

Since searches for brown dwarfs, close companions to bright stars, and envelopes around bright objects are amongst the most popular projects for AO systems, the camera is equipped with a cold coronograph, consisting of several interchangeable occulting masks and their corresponding Lyot-stops. To allow for very short integration times or on-line image selection, the camera will have a fast, cryogenic shutter. Image shifts due to mechanical flexure between the AO bench and the camera will be corrected via a laser-light reference point emanating from a separate window of the dewar.

The following sections discuss the individual components in detail.

2. SYSTEM COMPONENTS

2.1. The reflective optical system

We designed PHARO's optical system to maximize the throughput over the widest possible wavelength range, produce a sufficiently large pupil for spectroscopy, and use a minimum number of optical elements. The optical path includes two off-axis paraboloid (OAP) mirrors, plus two flat fold mirrors to minimize the overall dimensions of the system. One of three OAP camera mirrors can be placed in the collimated beam to select the low or high resolution imaging mode or a pupil imaging mode. For example, figure 1 shows a ray-trace for the 0.025"/pixel scale mode using a 486 mm focal length camera mirror.

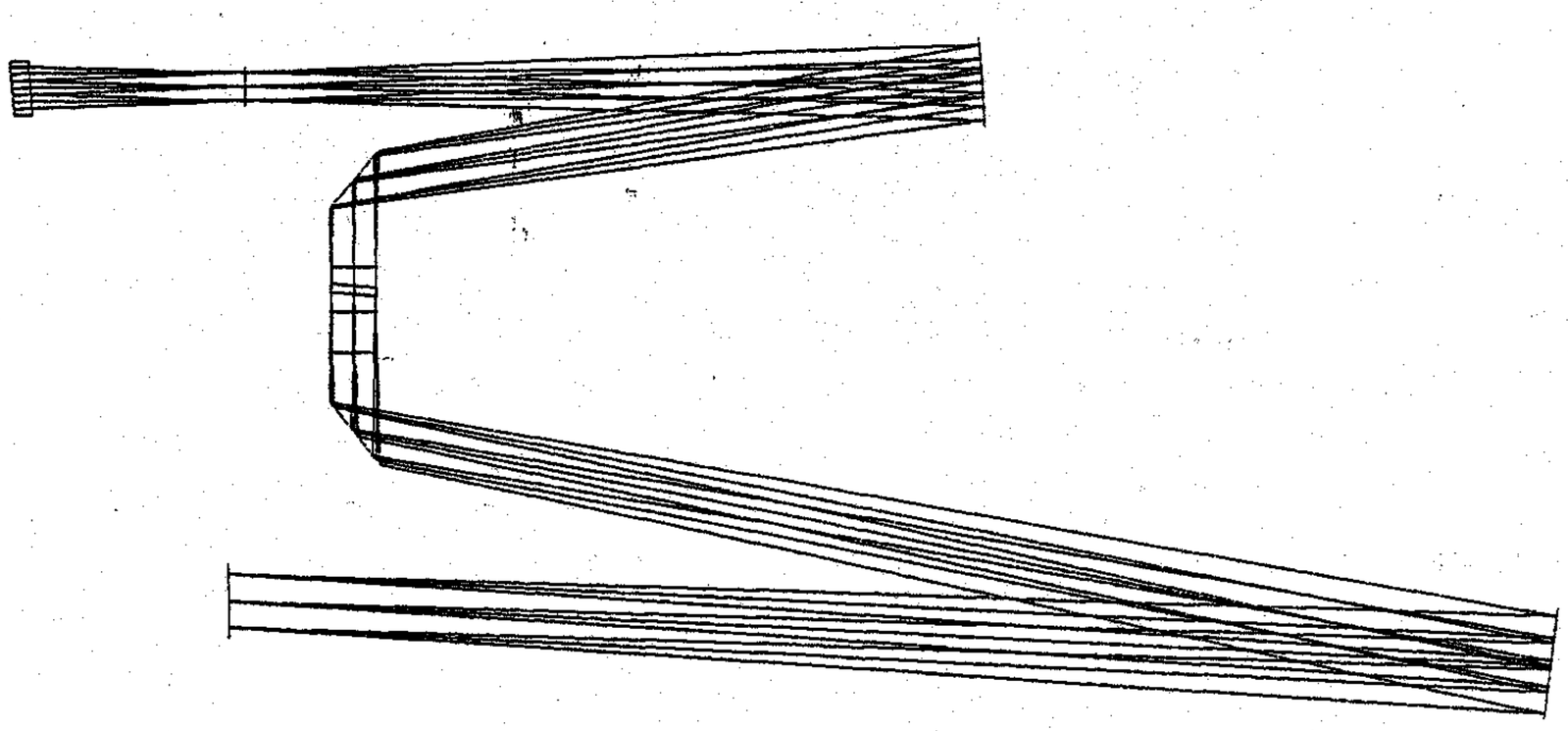

Figure 1 Ray-trace for the 0.025"/pixel optical system. The dewar window is in the left upper corner, followed by the object plane; the two OAPs are the elements on the right side, the image plane is in the lower left corner.

Changing to the low-resolution imaging scale is accomplished by inserting an OAP with focal length 303mm into the beam between the high-resolution mode OAP and the image plane. The magnifications are –1.91 and –1.19 for the 0.025"/pixel and 0.040"/pixel scales, respectively. The optical axis in this simple scheme is not perpendicular to the detector plane, but is tilted by -0.1° for the 0."025/pix-scale and 0.7° for the 0.040"/pixel scale. For geometrical reasons, minimizing the tilt angle is equivalent to maximizing the distance between the image plane and the OAP, which sets the upper limit for the coarser pixel scale.

Both imaging modes provide diffraction limited performance (>80% Strehl ratio) over the entire field of view and a Strehl ratio of >95% out to the edges of the detector. Image distortion is an aberration which cannot be completely eliminated in our simple system, but is rather small: two pixels in one dimension and eight pixels (0.8%) in the second dimension due to non-rotational symmetry. Figure 2 shows the expected Strehl ratio for the 0.040"/pixel scale as a function of the field of view.

The entire system of telescope-AO-system-camera has three pupils within the imaging path: the telescope mirror, the deformable mirror, and the camera stop. The alignment of the pupils is critical for minimization of background and scattered light, so we incorporated a third imaging mode into our design that allows direct imaging of the pupil onto the detector. This mode also allows the status and alignment of the Lyot-stop mask, shutter blade and filter wheels near the pupil to be easily checked. However, this mode need not be diffraction-limited, so just one optical element, an off-axis mirror with a conic constant of $c \approx -0.05$, provides good image quality.

Lumonics Optics (Nepean, Ontario) manufactured the aluminum diamond-turned OAPs with high surface quality. The flat mirrors are off-the-shelf Zerodur mirrors from Janos. According to the interferometric measurements of the manufacturers the combined wave-front error from the two OAPs and two flats is only 35 nm. All mirrors have been coated with protected gold.

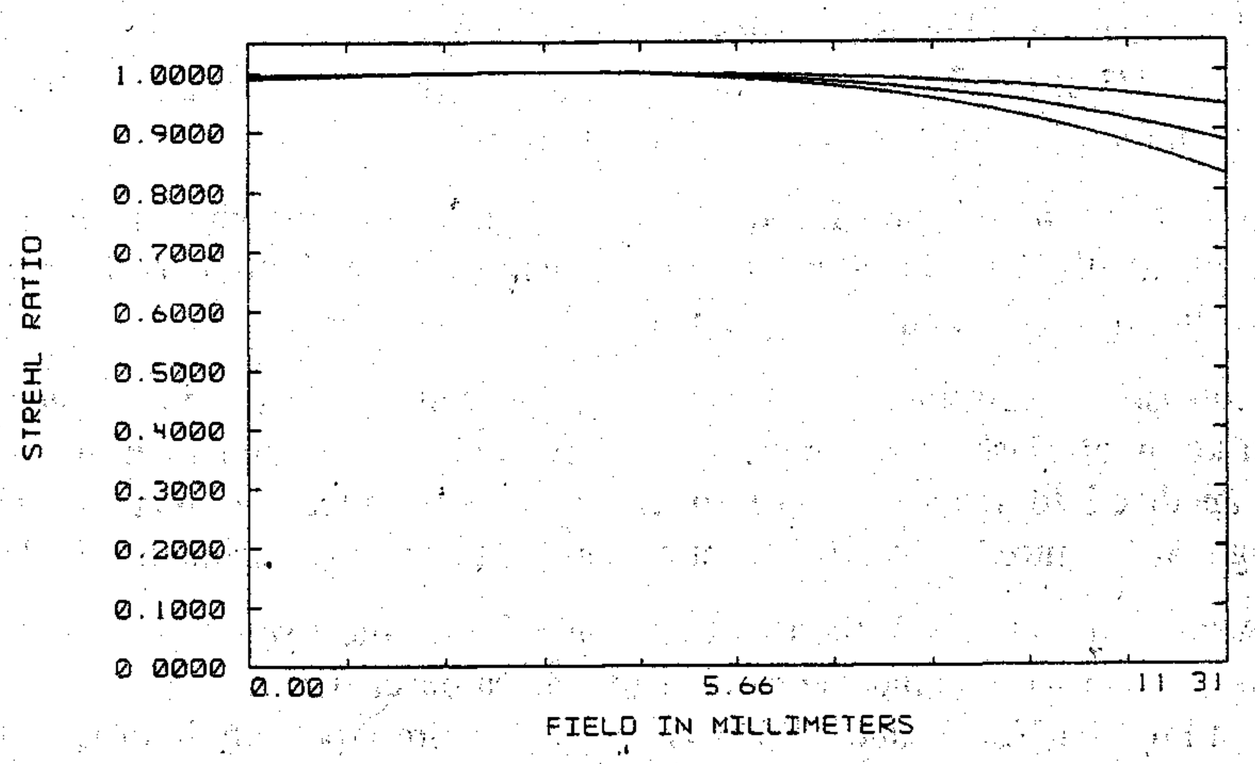

Figure 2 Expected Strehl ratio for the 0.040"/pixel optical system. The three curves represent the central wavelengths in J (1.25μm), H (1.65μm), and K band (2.20μm) from bottom to top. Note that the Strehl ratio is greater than 95% out to the edges of the array (corresponding to 8.0 mm field size in the object plane).

2.2. Grism spectroscopy

The relatively large pupil diameter of 16.12 mm enables high resolution spectroscopy using a grism. The grisms are mounted in a second filter wheel, close to the camera pupil, and thus can be used with either one of the image scales. They work in the first order of diffraction with about 180 rules/mm and prism angle ≈ 25°. We've chosen S-TIH10, an Ohara glass with refractive index $n \approx 1.7$, for the H- and K-band grisms; the J-band grism has not yet been designed. The index of this glass is a good compromise between the high index needed to minimize the blaze angle and the lower index desired to match the index of the resin used for the grating replica.

To provide the high spectral resolution also for extended sources and to avoid confusion with multiple sources in the field of view the camera is equipped with several slits, ranging from 50 μm to 200 μm slit width; the 50 μm slit width corresponds to 0.13" and provides $\lambda/\Delta\lambda \approx 1500$. All slits are mounted in the slit wheel in the focal plane. Due to the large number of pixels (spectral elements) of the HAWAII array, the spectra will span the full width of the J, H, or K atmospheric windows at this resolution.

2.3. Flexure compensation

Accurately centering a source on a 50 μm wide slit over a long period of time through varying zenith angles is a challenging task: optical components of the AO system which are not included in the correction loop and the science camera with its mechanical interface may be sources of tiny but significant flexure. Therefore we feed a laser light source into the dewar through an optical mono-mode fiber with 50μm inner diameter. The output end of the fiber is mounted beside the slit wheel and serves as a reference point that can be viewed through a separate window. This spatial information will be evaluated by the AO system so that detected shifts of the focal plane can be corrected in real time.

2.4. Other opto-mechanical components

Since the optical system consists of reflective elements, ghost images should be minimal. However, reflections can occur within or between the window, the filters, and substrates for the masks. Therefore, the window and mask substrates are made of CaF2 and are anti-reflection coated, providing an average transmission of 98% between 1.0μm and 2.5μm. Because the camera window is 3 inches in front of the AO focus, dust particles on the outer window surface will be blurred to ~1/3 of the field size avoiding sharp "artifacts". All filters are tilted by 5° (their design operating angle), more than the 3° needed to eliminate filter reflections.

All windows and substrates have been manufactured and coated by Janos. The broadband filters are currently being manufactured by OCLI especially for adaptive optics instrumentation, with tight constraints on surface parallelity (< 5"), flatness (λ/10 at 0.633 μm), and other parameters.

PHARO's coronograph mode consists of occulting masks in the focal plane and undersized Lyot-stop masks in the pupil plane, all at 77K. Both kinds of masks are mounted in wheels and have several interchangeable options. Some of the masks will be apodized to reduce diffraction effects and enhance the image contrast. These components are currently being manufactured at Deerfield Optics, Gurley Precision Instruments, and Lenox Laser.

There are four wheels in PHARO: the slit wheel, the two filter wheels, and the Lyot-stop wheel. Each of them hosts up to 10 filters or masks. These wheels and the camera mirror carousel will be driven by stepper motors inside the dewar. We've chosen Phytron VSS33 and VSS43 motors which are especially built for UHV cryogenic applications. The motors have a full step angle of 1.8° and a torque of about 40 mNm and 180 mNm, respectively, at 77K. They will be driven by Anaheim TM3000 bi-level driver boards mounted directly outside the dewar.

The use of a fast, cold shutter is desirable for two reasons:

1. Since the readout time for the entire detector is limited to ≈ 1s, a fast shutter can provide the shorter integration times desired for bright objects.

2. The correction efficiency of the AO system might vary during a long integration. The AO system can command the shutter to close it temporarily during periods of poor correction, eliminating the need to read and reset the detector before an optimal integration time (to minimize read noise, for example) is achieved.

Both applications require a compact shutter with negligible heat dissipation. We've chosen the Ascap AM1524 stepper motor, a tiny motor (15 mm in diameter) with 8 mNm torque and a step angle of 15°. The motor is available in a cryogenic version with "special aerospace lubricated ball bearings". Tests in our lab have shown that the motor runs reliably at 77K and produces sufficient torque to drive the shutter blade. Its power dissipation under (unrealistic) continuous operation with 6V at 77K is only 0.5Watts.

Figure 3. sketches the basic outline of PHARO's opto-mechanical setup on the cold work surface.

2.5. Dewar

The custom designed dewar was manufactured by Precision Cryogenics Systems, Inc. and is constructed almost entirely of 6061-T6 aluminum. Figure 3 shows two views of the dewar design. Although all interior components will be cooled to 77K, the dewar has two separate LN2 cans, one coupled to the work surface, the other to the radiation shield. The dewar is designed to permit LN2 cool-downs and refills while it is mounted to the AO bench with the filling tubes pointing toward the floor. The work-surface is held by four G-10 fiber-glass tabs; our flexure analysis has shown that the expected flexure of a single tab under full load is less than 40 μm. We also performed a finite element analysis to study the flexure of the dewar outer shell under various loads and tilt angles. In any case the total flexure was less than 3 μm.

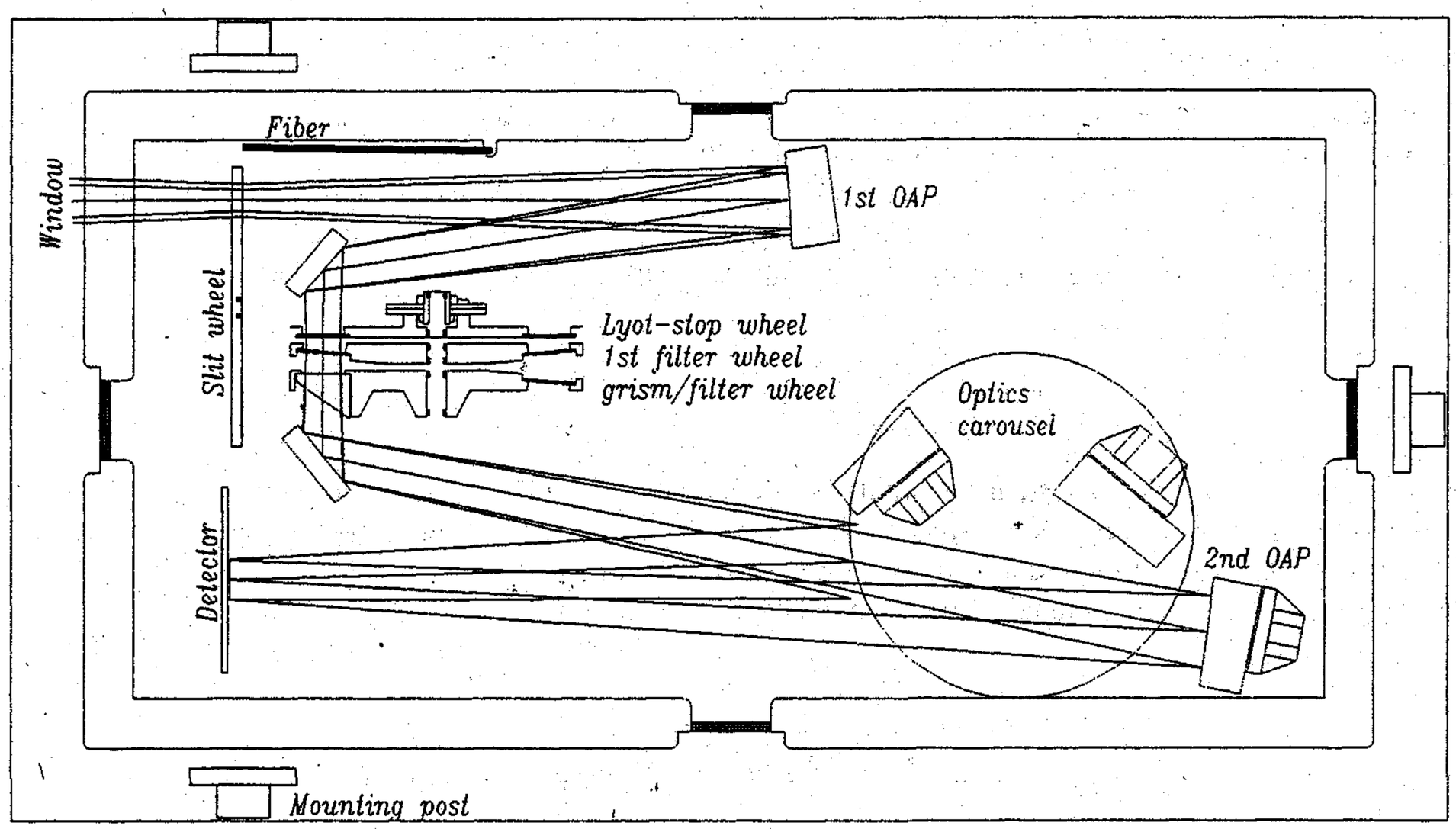

Figure 3: Sketch of the opto-mechanical setup of PHARO: the beam enters the dewar through a window close to the left upper corner and is focused at the slit-wheel; the beam the diverges and gets collimated at the first OAP in the upper mid section. Before the pupil the beam is folded and passes through the Lyot-stop wheel and two subsequent filter wheels, the latter of the two hosts the grisms. The nominal pupil position is in the Lyot-stop wheel. The beam gets re-imaged onto the detector by three OAPs, one of them in a fixed mounting (0.025"/pixel) and two on the optics carousel (the 0.040"/pixel camera mirror left and the pupil imaging mirror right). The drawing also shows the radiation shield, the outer boundaries of the dewar and the three mounting posts as well as the end of the fiber for the position reference point source.

2.6. HAWAII detector

PHARO's 1024×1024 pixel HgCdTe array is sensitive to 2.5 μm. The pixel pitch is 18.5 μm resulting in a square size of 19×19 mm. The device is subdivided into 4 quadrants, 512×512 pixels each which are linear up to ≈ 80,000 electrons; the quantum efficiency is ≈ 60%[3]. The read noise in a single read operation is about 15 electrons and can be further reduced by multiple, non-destructive reads[4], and the dark current is less than 0.1 electron/s. In comparison to NICMOS III 256×256 pixel arrays, this detector has a smaller pixel size, significantly lower read-out noise, and reduced residual images from previous exposures.

2.7. Detector electronics

The detector electronics consist of four separate boards. The device driver, preamplifier, and A/D boards, which were designed specifically for operation of the Rockwell HAWAII arrays, were purchased from the University of Hawaii Institute for Astronomy. The A/D's are 16-bit, 1 MHz devices, so we can cover the detector's entire dynamic range at a single gain setting. The measured electronics system noise is ~1.3 ADUs, well below the expected detector noise, and the system readout rate will also be detector-limited. The fourth board, which will provide overall detector clocking and control, is being custom-built at Cornell. It will combine a Field Programmable Gate Array (FPGA) with SRAM memory and a dual fiber-optic interface on a single board. Detector clocking tables and other control signals will be uploaded through one fiber optic channel into the on-board memory. During long integrations individual detector reads can be co-added in a second memory bank. Array data will be transmitted back to the control computer via the second fiber link.

2.8. Computer System

We plan to use a Sun UltraSparc station as the control computer. It will contain an Sbus card with a built in fiber-optic interface connected to the FPGA control board at the dewar and direct memory access (DMA) to the computer's system memory for efficient transfer of large blocks of data. A second video card and monitor will permit continuous display of a full 1024×1024 pixel image. Software will be written using Sun's GUI development tools following practices developed for Cornell's previous Palomar instrumentation[5].

3. SYSTEM SENSITIVITY

Figure 4 displays the calculated system sensitivity for the detection of a point source at the 10σ level in all three wavebands plus in the Bracket-γ line. Since some values (e.g., expected Strehl ratio, detector performance or surface reflectivities) involve large uncertainties, we used very conservative estimates for these numbers. Thus the system sensitivity might turn out to be higher than displayed in Figure 4.

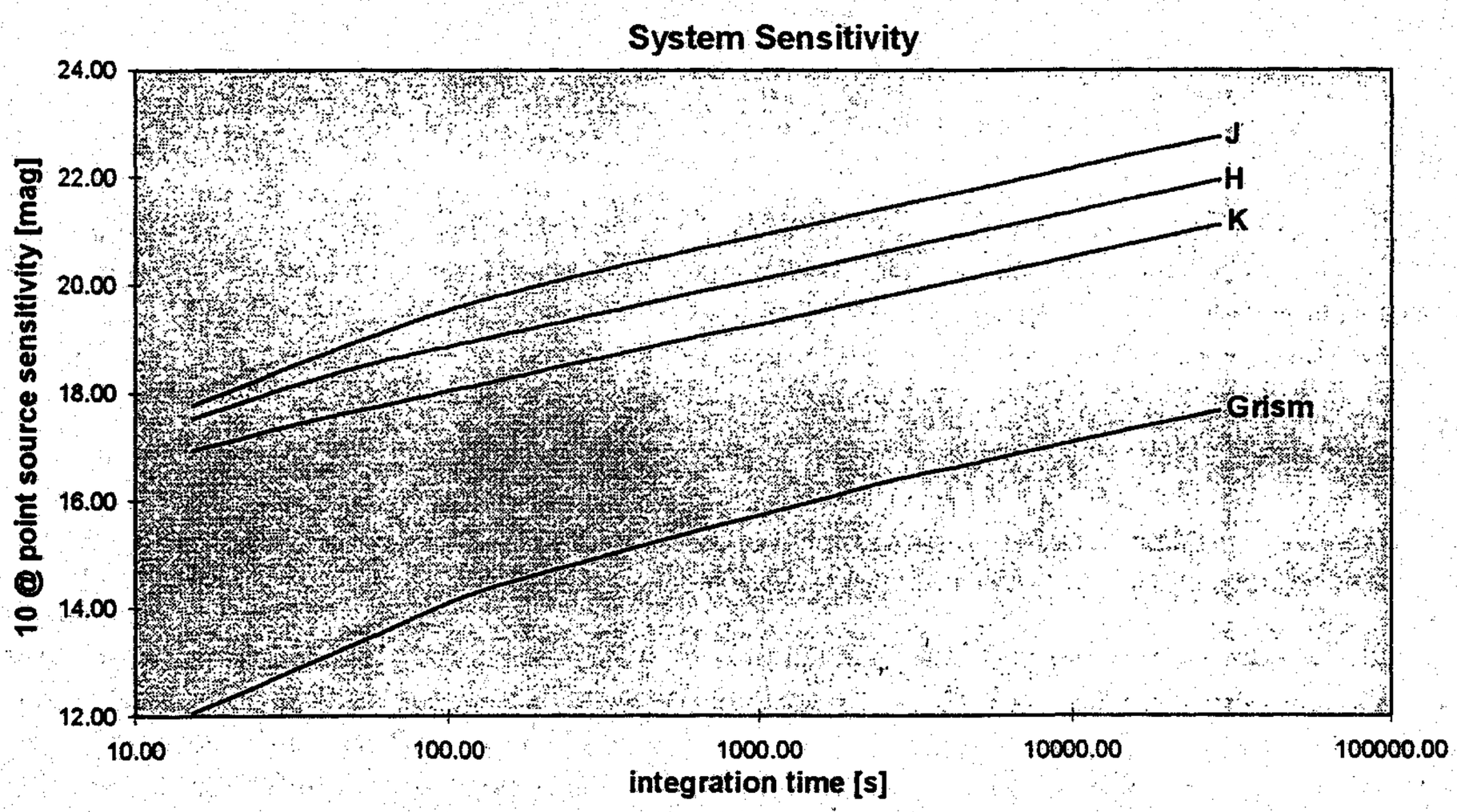

Figure 4: Predicted system sensitivity in the J, H and K-band and in the Brγ-line.

4. SUMMARY

We discussed most components of Cornell's NIR camera system for the 200" Hale telescope. We have shown that the concept is ideally suited to the scientific requirements of the Palomar adaptive optics system. It offers several interesting options, such as spectroscopy and coronography as well as imaging with different pixel scales. As this paper is presented work on the camera is still on goingn and some details might be subject to change. First astronomical light is expected in December 1997. A detailed description of the camera's performance will be presented in a subsequent paper.

ACKNOWLEDGEMENTS

This work wouldn't have become possible without a generous grant from the Norris Foundation and additional funding from the NSF under contract #AST-9601507.

REFERENCES

1. R. G. Dekany, A. Sivaramakrishnan, G. Brack, J. K. Wallace, B. Oppenheimer, D. Palmer, "Initial test results from the Palomar adaptive optics system", in *Adaptive Optics and Applications*, R. K. Tyson, ed., *Proc. SPIE* **3126**, pp. this volume, 1997.
2. B. Brandl, J. D. Smith, J. Wilson, F. Eisenhauer, and J. Houck, "Adaptive optics high spectral resolution imaging of the planetary nebula IC418", in *Adaptive Optics and Applications*, R. K. Tyson, ed., *Proc. SPIE* **3126**, pp. this volume, 1997.
3. L. J. Kozlowski, K. Vural, S. C. Cabelli, C.Y. Chen, D. E. Cooper, G. L. Bostrup, D. M. Stephenson, W. L. McLevige, R. B. Bailey, K. Hodapp, D. Hall, and W. E. Kleinhans, "2.5 μm PACE-I HgCdTe 1024×1024 FPA for infrared astronomy", in *Infrared Spaceborn Remote Sensing II*, M. S. Scholl, ed., *Proc. SPIE* **2268**, pp. 353-364, 1994.
4. K.-W. Hodapp, J. L. Hora, D. N. B. Hall, L. L. Cowie, M. Metzger, E. Irvin, K. Vural, L. J. Kozlowski, S. A. Cabelli, C.Y. Chen, D. E. Cooper, G. L. Bostrup, R. B. Bailey, D. Hall, and W. E. Kleinhans, "The HAWAII infrared detector arrays: testing and astronomical characterization of prototype and science-grade devices", *New Astronomy* **1**, pp. 177-196, 1996.
5. T. L. Hayward, J. W. Miles, J. R. Houck, G. E. Gull, and J. Schoenwald, "SpectroCam-10: a 10μm spectrograph/camera for the Hale telescope", in *Infrared Detectors and Instrumentation*, A. M. Fowler, ed., *Proc. SPIE* **1946**, pp. 334-340, 1993.